CrystEngComm

Accepted Manuscript

ROYAL SOCIETY OF CHEMISTRY

www.rsc.org/crystengcomm

One of the first reports of shape-controlled uranium oxides with hierarchical structure and their mechanism of formation.

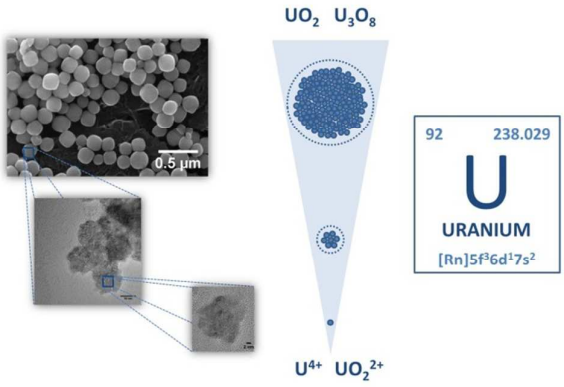

Preparation and characterisation of uranium oxides with spherical shape and hierarchical structure

G.I. Nkou Bouala [1], N. Clavier [1,], R. Podor [1], J. Cambedouzou [1], A. Mesbah [1], H.P. Brau [1], J. Lechelle [2], N. Dacheux [1]*

[1] ICSM, UMR 5257 CEA/CNRS/UM2/ENSCM, Site de Marcoule – Bât. 426, BP 17171, 30207 Bagnols/Cèze cedex, France

[2] CEA/DEN/DEC/SPUA/LMP, Site de Cadarache – Bât. 717, 13108 St-Paul lez Durance, France

*** Corresponding author :**

Dr. Nicolas CLAVIER

ICSM – UMR 5257 CEA/CNRS/UM2/ENSCM

Site de Marcoule – Bât 426

BP 17171

30207 Bagnols sur Cèze

France

Phone : + 33 4 66 33 92 08

Fax : + 33 4 66 79 76 11

nicolas.clavier@icsm.fr

Abstract :

An easy way of preparation, based on the precipitation of U^{4+} or UO_2^{2+} cations by urea in presence of PEG at T = 90-120°C, was set up to prepare shape-controlled spherical uranium oxides. Parametrical study of heating time and temperature allowed to tailor the size of the mesocrystals obtained, which varied from 50 to 250 nm. For U(IV)-based samples, advanced characterization thanks to the combination of SEM and HR-TEM observations, PXRD and SAXS measurements revealed a hierarchical organization of the powder with three different levels. The first one corresponded to small crystallites of about 3 nm, which grouped into spherical agglomerates of 15-20 nm then again aggregate to produce the bigger spheres observed (up to 200 nm in diameter). On the other hand, U(VI)-bearing spherical aggregates were found to be more likely a meta-stable form, evolving towards the precipitation of crystalline meta-schoepite. In a last step, the samples prepared at low temperature were fired between 700 and 1000°C under various atmospheres in order to tailor the final O/M ratio in the resulting oxides. In spite of the important chemical modifications associated, the precursors were generally found to present pseudomorphic conversion towards the final high temperature oxides, and still exhibited a spherical habit, provided the conditions of calcination were properly selected.

1. Introduction

For decades, self-assembly of nanoparticles leading to the formation of superstructures with well-defined shapes is getting more and more interest in the literature [1]. These objects are frequently depicted under various appellations including superparticles [2], mesocrystals [3] or hierarchical materials [4], but all result from the aggregation of nanometric crystallites into bigger structures through the action of molecular interactions, i.e. van der Waals, Coulombic or hydrogen bonding, that differ from usual covalent, ionic or metallic bonds [5]. Among several other compounds, the control of the morphology of the final assembly takes on a great importance for oxides and hydroxides based materials as it could lead to significant modifications in their behaviour. Particularly, monitoring the shape of inorganic materials could be considered as a promising way to tailor several physico-chemical properties of importance in various applications such as catalysis [6] or electrochemistry [7].

Although they are far less mentioned in the literature, the need of shape-controlled oxides also constitutes a great challenge for actinide-based materials [8], and more specifically for uranium oxides. As instance, uranium oxide nanospheres have already attracted some attention in view of their catalytic properties, particularly in the framework of the destruction of volatile organic compounds [9]. More importantly, as uranium oxide constitutes the reference fuel for the current nuclear reactors and for several future Gen IV concepts [10], the design of spherical uranium oxides with tailored size could allow the preparation of powders with interesting properties, such as improved flowability [11, 12]. Also, such nano-, meso- or micro-spheres could appear as helpful models to study various processes involved in the fabrication of nuclear fuel, and particularly the early step of sintering of ceramic pellets.

In this framework, the precipitation of uranium oxide precursors through sol-gel processes was reported for long, and usually produced spheres in the range of 100 to 500 µm [13, 14]. On an opposite scale, some more recent works demonstrated the possibility to prepare uranium oxide nanospheres (typically from 1 to 5 nm) through non-aqueous synthesis in highly coordinating organic media [15, 16]. Hence, there seems to be a lack of data concerning the preparation of uranium oxides with controlled shape, and particularly spherical objects, at the mesoscale, i.e. from about 10 to 100 nm, which is the classical domain of size obtained for hierarchical structures. On this basis, this study reports the design of uranium-based mesospheres *via* the initial preparation of precursors through simple aqueous precipitation of either U^{4+} or UO_2^{2+} cations. The influence of several parameters impacting directly the final shape and size of the superstructures obtained, such as temperature or heating time, will also be examined. Advanced characterization of the mesospheres by SAXS and HR-TEM will then be used to propose some insights on their mechanism of formation. Finally, the conversion of the precursors under oxidative or reducing atmospheres will be investigated in order to obtain uranium oxides with tailored O/M ratios.

2. Experimental

Chemicals. All the reagents used were of analytical-grade and supplied by Sigma-Aldrich, except uranium sources. The preparation of uranium tetrachloride solution was performed by dissolving uranium metal in hydrochloric acid. The metal pieces were first washed in 2M HCl in order to eliminate possible oxide traces present at the surface, rinsed with water and ethanol and finally dissolved in 6M HCl. Such high chloride concentration allowed us to maintain the tetrapositive oxidation state of uranium in solution for several months [17], thus avoiding possible bias coming from the presence of U(VI) in the reacting media. The uranium concentration of the final solution was estimated to 0.74 ± 0.02 M using the titration method developed by Dacheux *et al.* [17, 18]. All the scraps coming from the preparation of U(IV) hydrochloric solution were further oxidized by dissolution in concentrated nitric acid. Uranium (VI) was then separated from impurities by adding H_2O_2 and precipitating meta-studtite ($UO_4.2H_2O$) [19]. This latter was finally dissolved again in fresh nitric acid to reach a final U(VI) concentration of 0.1 M.

Preparation of the samples. The synthesis of uranium oxides mesospheres was adapted from the protocol previously reported by Wang *et al.* [20] for the preparation of CeO_2 powders with controlled morphology. Such process is mainly based on mixtures of solutions containing the cations, urea as a precipitating agent, and a surfactant ensuring the spherical morphology of the final product.

During our study, two different methods were investigated, starting either from uranium(IV) in hydrochloric media or from uranium(VI) in nitric media. Even if the counter-anion was modified depending on the system considered, no significant difference was expected in terms of reactivity in solution, the thermodynamic constants of complexation of uranium versus NO_3^- and Cl^- being very close [21]. Thus, whatever the starting solution and redox state considered, 10^{-3} mole of uranium was first poured in 50 mL of PEG solution (2.10^{-3}M). The mixture was then aged for 30 minutes, before addition of 5g of urea. The precipitation was then finally performed by heating between 90 and 120°C, either on a sand bath or in an oven. All these steps were performed under magnetic stirring in order to maintain the precipitate in suspension.

For all the samples prepared, the solid phase was finally separated from the supernatant by centrifugation, washed several times with deionized water then ethanol, and finally dried overnight at 60°C in an oven.

SEM observations. Prior to their observation, the samples were dispersed in acetone and deposited on a vitreous carbon sample holder. Scanning Electron Microscope (SEM) micrographs were further directly recorded from the as-deposited powders without additional

preparation such as metallization. A FEI Quanta 200 environmental scanning electron microscope, equipped with an Everhart-Thornley Detector (ETD) and a Back-Scattered Electron Detector (BSED), was used to record images with an acceleration voltage of 30kV under high vacuum conditions.

PXRD. Powder X-Ray Diffraction (PXRD) diagrams were obtained by the means of a Bruker D8 diffractometer equipped with a Lynx-eye detector adopting the reflexion geometry, and using Cu $K\alpha_{1,2}$ radiation (λ = 1.54184 Å). PXRD patterns were recorded at room temperature in the $5° \leq 2\theta \leq 120°$ range, with a step size of $\Delta(2\theta) = 0.03°$ and a total counting time of about 1.5 hours per sample.

All the PXRD patterns were refined by the Rietveld method using the Cox-Hastings pseudo-Voigt profile function [22] implemented in the Fullprof_suite program [23]. During all the refinement, the conventional profile/structure parameters were allowed to vary, i.e. zero shift, unit cell parameters, scale factors, global thermal displacement and asymmetric parameters. Moreover, the modelling of the intrinsic microstructure parameters was performed for each phase by applying an anisotropic size model.

SAXS. SAXS experiments were performed in the transmission geometry, using a molybdenum anode delivering a wavelength of 0.71 Å. The monochromation was achieved using a Xenocs Fox2D multishell mirror. Two sets of scatterless slits allowed the beam to be collimated and to have a squared shape of side 0.8 mm. SAXS patterns were recorded on a MAR345 2D imaging plate, which enabled the simultaneous detection over scattering vectors q ranging from 0.3 to 10 nm^{-1}. *In situ* temperature SAXS measurements were performed using an oven specially designed for the SAXS set-up, in which glass capillaries can be used as sample holders. In such experimental conditions, the solid phase appeared to be suspended in solution during the first 2 hours of reaction, then settled down to the bottom of the capillary for longer durations.

TEM. Transmission Electron Microscope (TEM) observations were performed thanks to the advanced technology of the JEOL JEM-ARM200F who allowed unprecedented atomic scale analysis. This device combined a spherical aberration corrector CEOS™ and a cold field emission gun (CFEG) which allowed information transfer below 75 pm at 200 kV. These experimental conditions led to directly image the atomic arrangement of the samples along various indexes zone axis. Prior to the observations, samples were simply deposited on the grid in a solvent droplet after ultrasonic dispersion.

TG-DT Analyses. Thermogravimetric analyses were undertaken thanks to a Setaram Setsys Evolution equipped either with a type-S thermocouple (Pt / Pt-10%Rh) when working in air

or with W5 device (W-5%Re / W-26%Re) for analyses performed under reducing atmosphere. After recording of a baseline using an empty crucible (100 µL), weight loss was measured during a heat treatment up to 1000°C with a rate of 10°C.min^{-1}.

3. Results and discussion

3.1. Influence of time and temperature over size and morphology

The formation of uranium-bearing mesospheres was first investigated as a function of the heating time considered to perform the precipitation at 100°C. In such operating conditions, the kinetics of precipitation appeared to differ significantly depending on the starting solution used, then on the redox state of uranium. On the one hand, using hydrochloric U(IV) solution as uranium source led to the formation of a black precipitate after about 45 minutes. On the other, syntheses starting from uranium(VI) in nitric media systematically led to the precipitation of a yellow powder after only 25 minutes of heating.

On this basis, the SEM observations of the U(IV)-bearing samples performed after 1 hour of heating (Figure 1) revealed the formation of spheres of about 120 nm in diameter. Moreover, the powder could be almost considered as monodisperse since the variation in size of the spheres was found to be very limited. A prolongation of the heating time then did not lead to a significant increase of the spheres' size, which was still estimated around 120 nm. Nevertheless, from 1h30 of heating, the initial spheres start to agglomerate, leading to bigger particles that exceed 1 µm in length. This aggregation process was then pursued for longer heating times. Again, the resulting micrometric particles observed after 2 hours seemed to adopt a spherical habit. These observations thus confirm the capability of such easy way of synthesis to form hierarchical microstructures.

In parallel, the powdered samples were analysed through PXRD in order to evidence the nature of the solid obtained. Whatever the heating time considered, the patterns recorded for U(IV)-based compounds (Figure 2a) all exhibited the characteristic PXRD lines of a fluorite-type structure, even if the large FWHM accounted for a partly crystallized and/or nanosized solid. On this basis, the samples obtained were identified to hydrated uranium(IV) dioxide, $UO_2.nH_2O$. The formation of such nanosized and/or amorphous oxide at relatively low temperature probably resulted from the initial formation of colloidal UO_2 in the solution, which was already reported in the literature, either for synthetic samples or in natural systems [24, 25].

Moreover, the Rietveld refinement of the PXRD patterns allowed us to estimate the average size of the coherent domains, i.e. the size of the crystallites that constitute the elementary brick of the hierarchical structure, to about 3 nm. The hierarchical structure of the $UO_2.nH_2O$ particles then presented three different levels of organization. Indeed, the mesospheres of about 120 nm initially obtained already resulted from the self-organization of smaller nanoparticles, and then tend to form bigger aggregates when increasing the heating time. Also, heating time was not found to induce significant growth processes, as the crystallite size value was systematically found around 3 nm. Again, this result appears to be

consistent with the initial formation of small UO_2 colloids in the aqueous solution, followed by their aggregation into spheres.

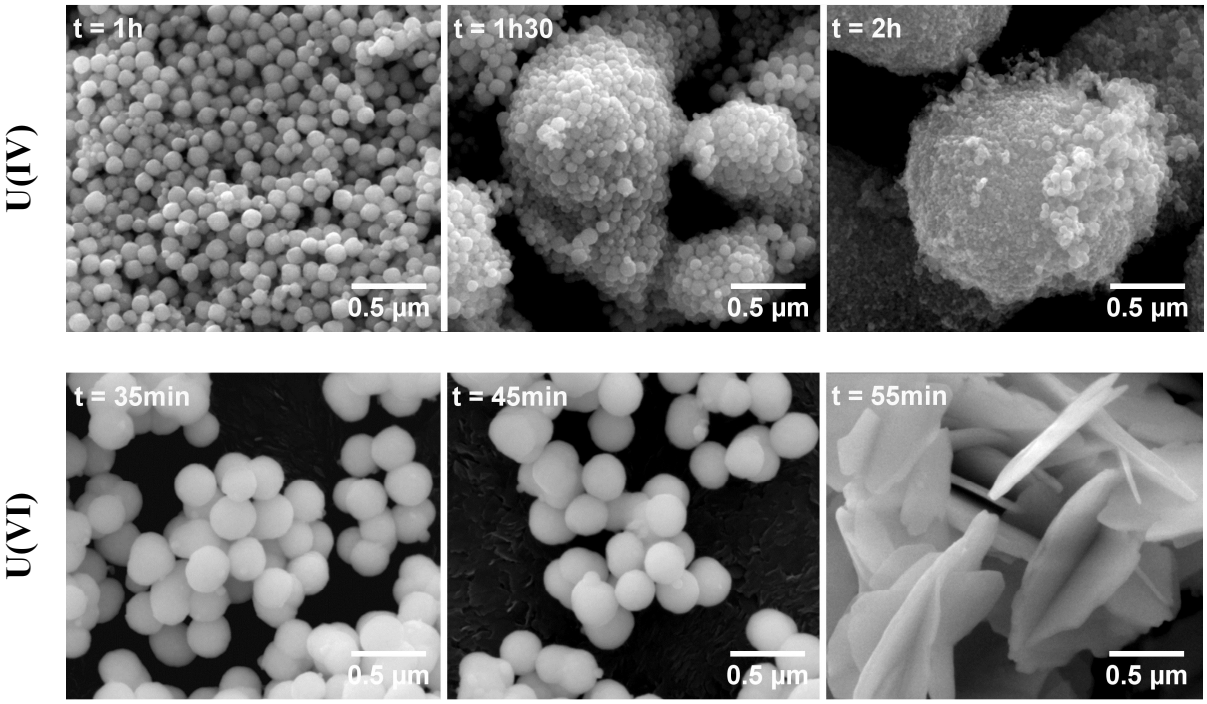

Figure 1. SEM observations of U(IV)- and U(VI)-bearing microspheres versus heating time at 100°C.

Samples obtained from the precipitation of uranium(VI) source exhibited a rather different behaviour versus heating time at 100°C. First, as already mentioned, precipitation occurred significantly faster, leading to the formation of spherical grains as soon as after 35 minutes of heating (Figure 1). Even though a significantly shorter precipitation time was considered, the size of the U(VI)-bearing superparticles was found to be twice that of $UO_2.nH_2O$ mesospheres, with an average value close to 250 nm in diameter. Again, the distribution in size appeared to be rather homogenous, resulting in a monodisperse powder. Such features were further conserved after 45 minutes, but appeared to be drastically modified when reaching 55 minutes of heating. For such operating conditions, the spherical superstructure of the particles was no longer observed and gave way to plate-like crystals arranged into "sand-rose" aggregates. These latter appeared to be bigger than the initial spherical particles and reached up to 3-5 µm in length.

This spectacular variation of the powder's morphology was also linked with important modifications in the PXRD pattern of the samples (Figure 2b). First, the spherical particles obtained between 25 and 35 minutes of heating at 100°C mainly corresponded to an amorphous material. In a similar way to what was observed for U(IV) samples, this could

argue for the initial formation of colloids in the solution, that frequently appeared to be poorly crystallized. Indeed, even occurring through a complex hydrolysis mechanism, the formation of colloidal U_3O_8 from UO_2^{2+} molecular ions was already described in the literature [26]. After 45 minutes, the apparition of a small and wide diffraction line at about 13° seemed to indicate the initiation of a crystallization process. This latter was confirmed by the apparition of sharp diffraction peaks on the pattern at t = 55 min., which were assigned to the formation of a mixture of ammonium uranate (with general formulae $(NH_4)_2U_2O_5.nNH_3$) [27, 28], schoepite [29] and meta-schoepite [30] ($[(UO_2)_8O_2(OH)_{12}](H_2O)_{10\text{-}12}$). On this basis, prolonging the heating time during the preparation of U(VI)-based samples did not result in an amplification of the aggregation processes, like for U(IV). Most likely, it probably induced a combination between hydrolysis and dissolution/precipitation mechanisms to reach the precipitation of crystallized phases.

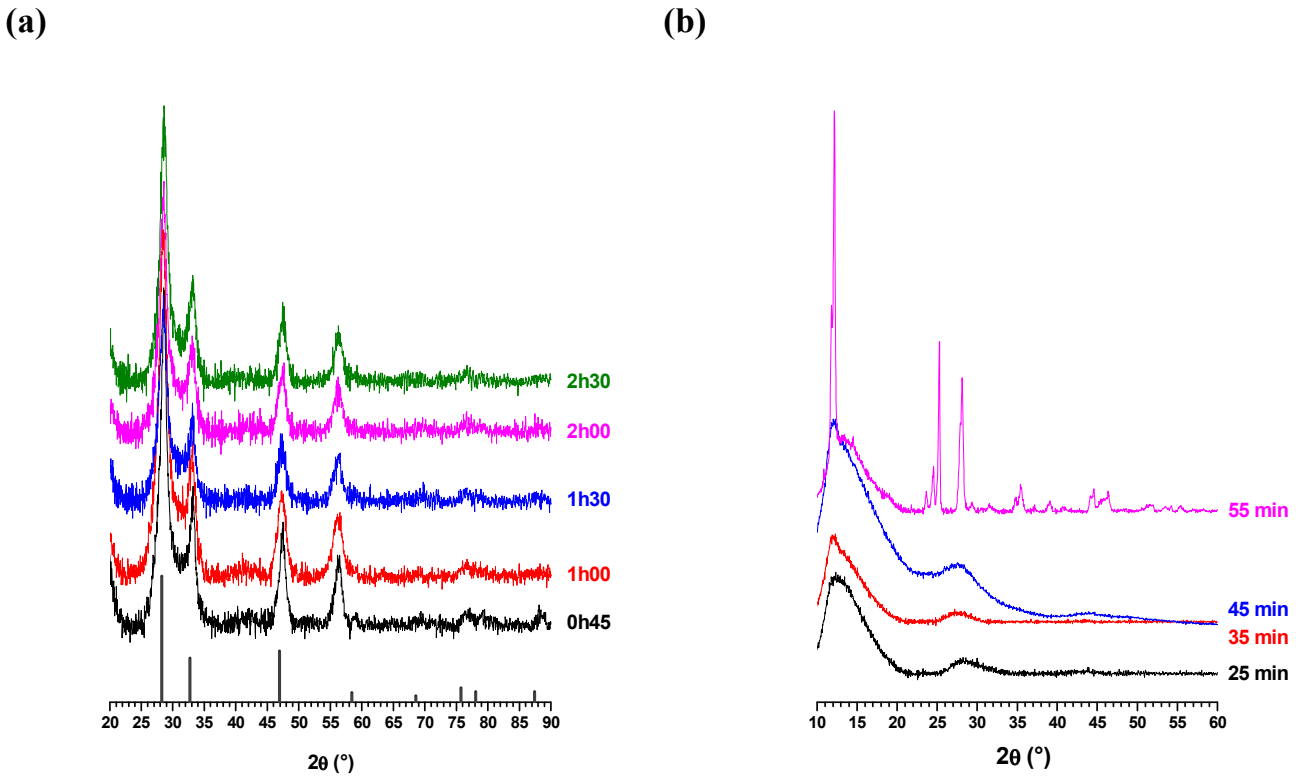

Figure 2. PXRD patterns of the samples prepared from U(IV)- (a) and U(VI)-bearing (b) solutions versus holding time at 100°C. Theoretical diffraction lines of UO_2 (JCPDS 071-6416)[31] are gathered for comparison purposes.

In a second step, the morphology of the samples prepared was investigated as a function of the temperature of precipitation in the range 90-120°C. In this purpose, the heat treatment duration initially considered, i.e. 1 hour for U(IV) compounds and 35 minutes for U(VI) samples, was conserved. Nevertheless, it was not found to be sufficient to reach the

precipitation of a solid phase at 90°C. For this lower temperature, heating times of 3 and 2.5 hours were achieved for U(IV) and U(VI) samples, respectively.

Conversely to the heating time, the temperature appeared to significantly modify the size of the $UO_2.nH_2O$ mesospheres (Figure 3). Indeed, their formation at 90°C resulted in the preparation of very small superparticles of about 15 to 20 nm in diameter, thus corresponding to the aggregation of a dozen of elementary crystallites. As previously evidenced, the size of these aggregates increased by a factor of 5 to 10 when heating at 100°C, and reached about 120 nm. Once again, this result indicated that the formation of U(IV)-bearing mesospheres is not driven by nucleation/growth mechanisms, but more likely by aggregation processes, that are usually encountered in self-assembly inorganic materials [5]. This tendency was then confirmed by the micrographs recorded on the samples prepared at 120°C for which the size reached up to 250 nm diameter. Nevertheless, this increase of the spheres' size also appeared to be accompanied by a moderate change of morphology, illustrated by slightly angular edges. The spherical shape of the superparticles then seemed to evolve to a cubic habit which should be the most stable one, owing to the fluorite-type structure of uranium(IV) dioxide.

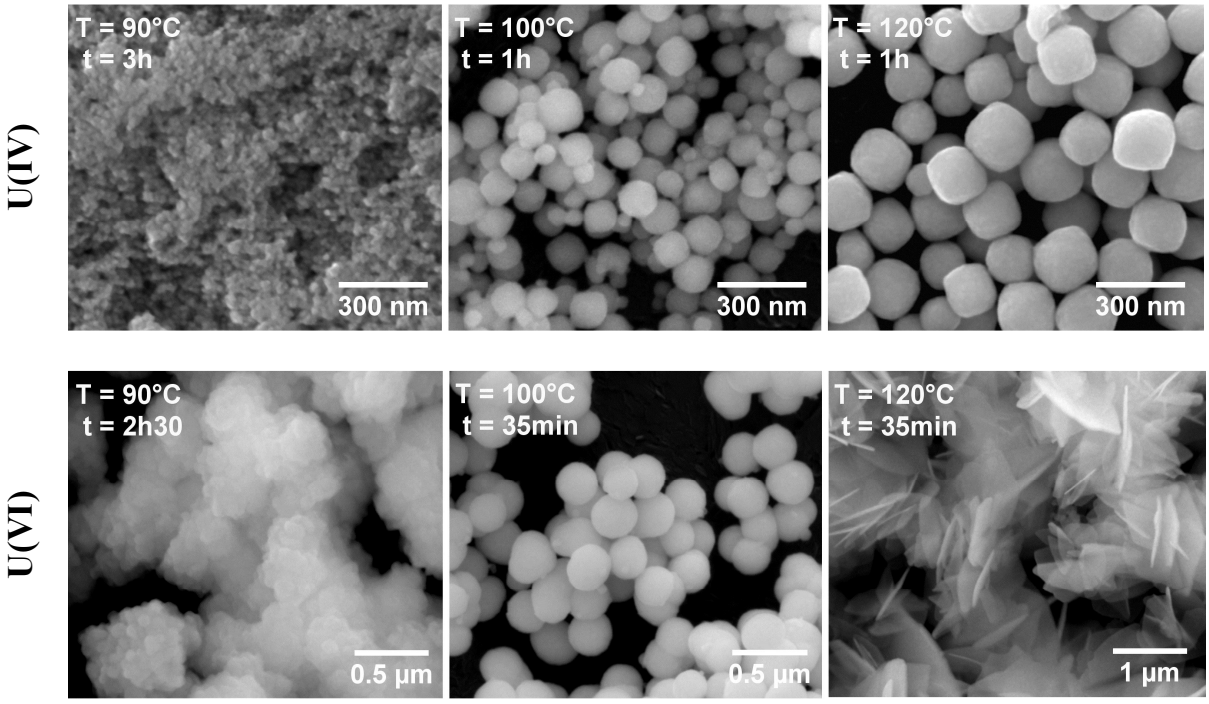

Figure 3. SEM observations of U(IV)- and U(VI)-bearing microspheres versus heating temperature. The minimal reaction time required to observe precipitation was considered for each temperature investigated.

In a similar way to what was stated when looking at the influence of heating time, the effect of temperature over the morphology of U(VI)-bearing samples was found to differ from

that of $UO_2.nH_2O$. Indeed, solely the temperature initially chosen to perform the preparation of shape-controlled U(VI)-based samples (100°C) allowed the formation of mesospheres. For lower temperatures, the important slow-down of the precipitation kinetics led to poorly defined grains of about 500 nm in length, composed of smaller nanoparticles. Conversely, increasing the temperature up to 120°C resulted in the early formation of sand rose-like aggregates that suggest the crystallization of schoepite, meta-schoepite and ammonium uranate. From these observations, the formation of the mesospheres thus appeared to be a transient step, which probably occurs during a progressive hydrolysis reaction leading from amorphous U(VI)-bearing colloids in solution to crystalline phases. Hence, in this particular case, neither the heating time nor the temperature could be used as a pertinent process parameter to monitor the size of the spherical particles obtained. However, such size control might be achieved by varying chemical parameters, and especially the initial concentration of surfactant within the reacting media.

3.2. Investigation of the aggregation mechanism

In order to obtain further insights into the formation mechanism of the mesospheres, *in situ* small angle X-ray scattering (SAXS) experiments were performed on the reacting media containing U^{4+} cations. After having measured the SAXS diagram of the starting mixture at room temperature (see the "0 min." pattern in Figure 4a), temperature was set at 90°C. Scattering patterns of the sample were then recorded every 20 minutes, which therefore corresponded to our time resolution (Figure 4).

After 20 minutes at 90°C, the SAXS profile appeared to be very close to that recorded from the unheated reacting media. No signal coming from nanometric objects was therefore detected. Conversely, a signal emerged at low angle after 40 minutes, and then grew until 120 minutes of heating at 90°C. Moreover, the shape of this signal slightly evolved with the heating time. In particular, a shift in the positions of oscillations towards smaller scattering vector values was observed. After 120 minutes of heating, the positions of the oscillations no longer evolved, but a progressive decrease of the signal at low scattering vectors was observed.

The signal observed at small angle values was thus fitted with a mathematical function reproducing the form factor of non-interacting spheres [32]. The sphere diameter was adjusted in order to get the best agreement between the numerical simulation and the experimental data. An example of such an adjustment is given as supplementary information for the spectra recorded after 120 minutes of heating (Figure S1). For each simulation, a Gaussian distribution of diameter was considered in order to take into account the polydispersity of the objects. For the 40 min. profile, the mean diameter of the spheres was found to be about 9 nm with a Gaussian distribution of full width at half maximum (FWHM) of 4 nm. Then, the mean

sphere diameter increased up to 13 nm (FWHM =5 nm) after 60 minutes and finally reached a nearly constant diameter of 16 nm (FWHM = 5 nm) after 80 minutes (Figure 5).

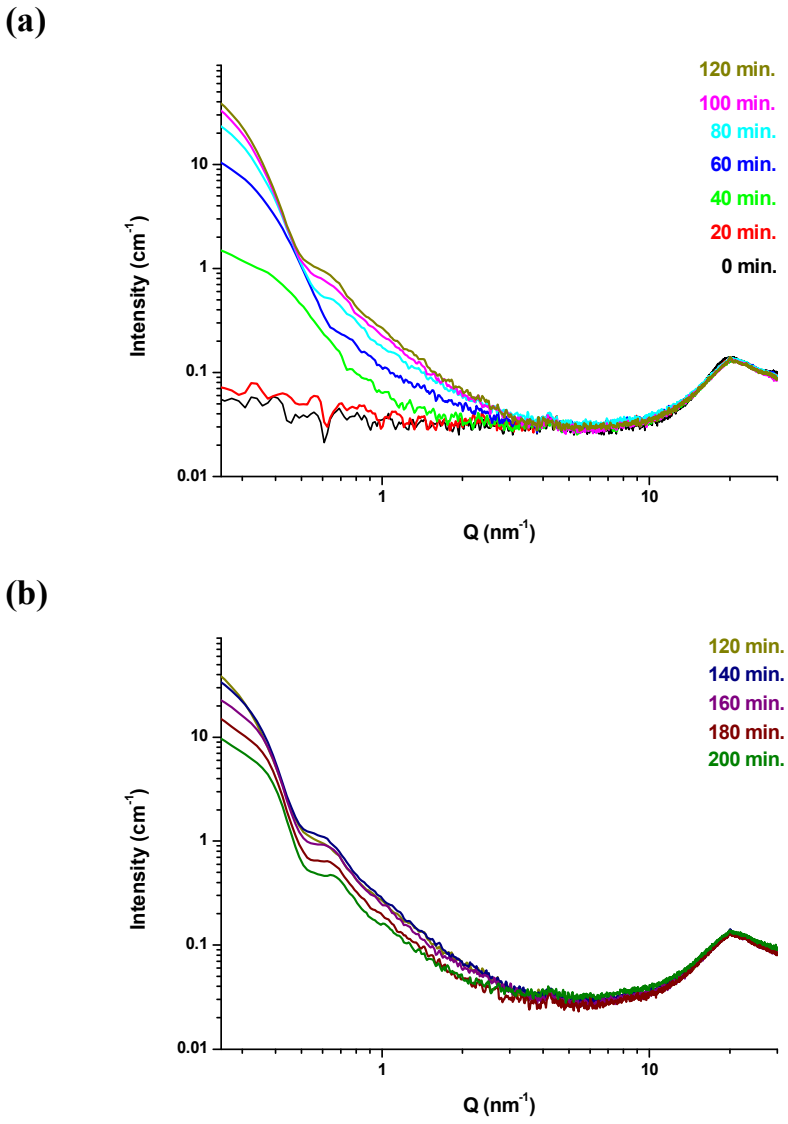

Figure 4. SAXS profiles of the starting mixtures at T = 90°C, recorded each 20 minutes between 0 and 120 minutes (a) and between 120 and 200 minutes (b). The diagram denoted "0 min." was recorded at room temperature.

Moreover, the fitting procedure performed allowed the measurement of the volume concentration of spherical objects in the reacting medium. The evolution of the number of spheres of mean diameter 16 nm is thus depicted in Figure 5 and clearly presented two distinct steps. During the first phase (between 40 and 120 minutes), a quick increase of the

number of spheres was observed until a maximum was reached after 120 minutes of heating. Also, it is important to note that only the spheres with a diameter of 16 nm were numbered, but spheres of smaller diameter were also detected after 40 and 60 minutes. Therefore, this first phase appeared to correspond to a "growth" regime, probably driven by the aggregation of the elementary crystallites previously evidenced by Rietveld refinement of the PXRD patterns. During the second phase, the size of the spheres no longer evolved. Moreover, one can observe a linear decrease of the spheres concentration in the sample. Such evolution could be related to the progressive sedimentation of the spheres to the bottom of the sample holder. The spheres thus progressively exit the probed volume and settled down. Small amounts of powders were indeed visible at the bottom of glass capillaries at the end of the experiment. This phase could then be illustrated as the "sedimentation" of the 16 nm mesospheres initially formed from the elementary crystallites. Similar process might also have occurred during the first phase, but was probably less significant and hindered by the growth of the aggregates.

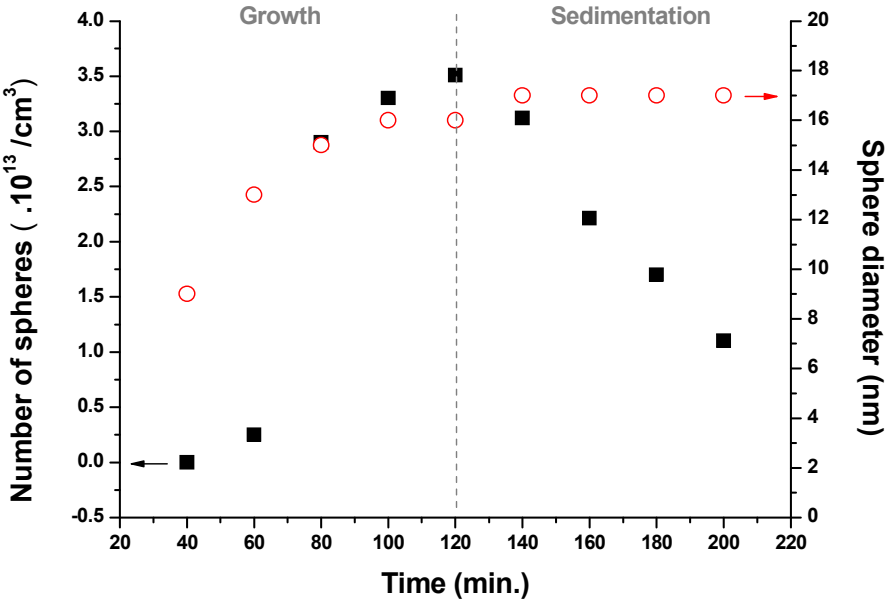

Figure 5. Evolution of the volume concentration of $UO_2.nH_2O$ mesospheres with diameter ≈ 16 nm (■) and of the mean sphere diameter (o) in the synthesis medium.

The hierarchical structure suggested by combining PXRD and SAXS analyses was finally verified by performing HR-TEM observations of the U(IV)-based samples prepared at 90°C (Figure 6). The micrographs recorded with an atomic resolution revealed several scale of organization which appeared in good agreement with the results previously exposed. First, the existence of small coherent domains was clearly evidenced by the presence of numerous

lattice fringes (see green circle on Figure 6), resulting in a crystallite size close to the value of 3 nm determined through PXRD. These crystallites themselves arranged into bigger particles (blue circle), of about 10 to 20 nm in diameter. Such objects probably constitute the spheres detected during SAXS measurements. Also, one can note that both single mesospheres and aggregates built from several of them were evidenced. This tendency to the aggregation then probably contributed to the sedimentation step evidenced by SAXS. Moreover, these observations again confirm the assumption previously evocated concerning an higher level of organization, that led to spherical objects with sizes typically varying from 100 nm to 1 µm, depending on the heating time and temperature considered. Finally, EDS analyses coupled to the HR-TEM observations also permitted to reveal the presence of carbon as residual organic material inside the aggregates (see the orange insert in Figure 6). This latter probably originates from the presence of PEG as a surfactant in the initial reacting mixture, and was not fully eliminated by the various washing steps performed.

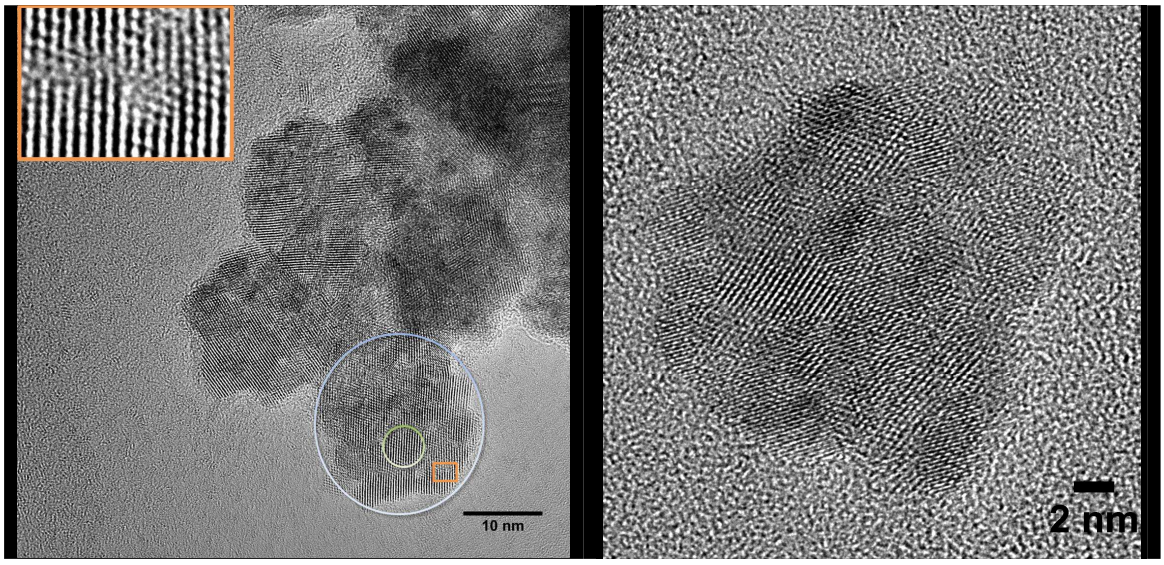

Figure 6. HR-TEM observations of the U(IV)-bearing samples prepared after heating for 3 hours at 90°C. The dimensions of the zone detailed in insert are 5.12 × 3.65 nm.

3.3. Conversion toward uranium oxides

In order to finally perform the preparation of uranium oxides with controlled morphology, the conversion of the precursors synthesized was performed through a heat treatment at high temperature. In this purpose, two different atmospheres of calcination were considered, i.e. air and reducing Ar/H_2, to tailor the final O/M ratio of the oxides.

The transformation of the two precursors prepared into final oxide samples was first investigated through thermogravimetric analyses (Figure 7). For mesospheres obtained from uranium(IV) solution, similar behaviour was observed when working under reducing or oxidative atmospheres. Under Ar/H_2, a progressive weight loss of about 6% of the initial mass was observed when heating up to 400°C, and was assigned to the departure of one water molecule leading to anhydrous UO_2. On this basis, and considering the results obtained from the XRD characterization of the precursor sample, the initial formulae of U(IV)-bearing mesospheres could be written as $UO_2.H_2O$.

(a)

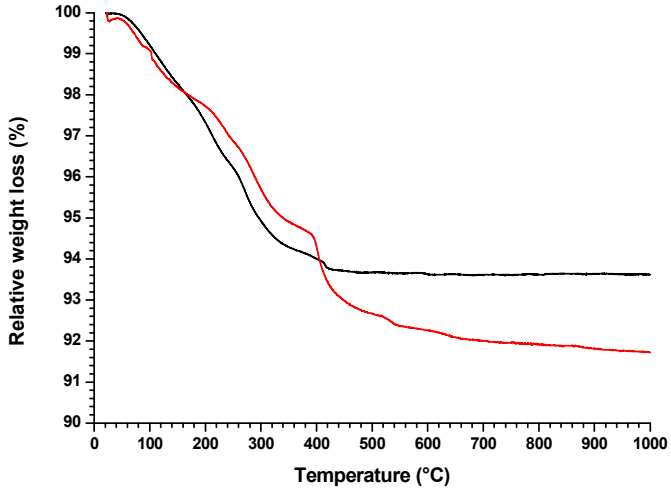

(b)

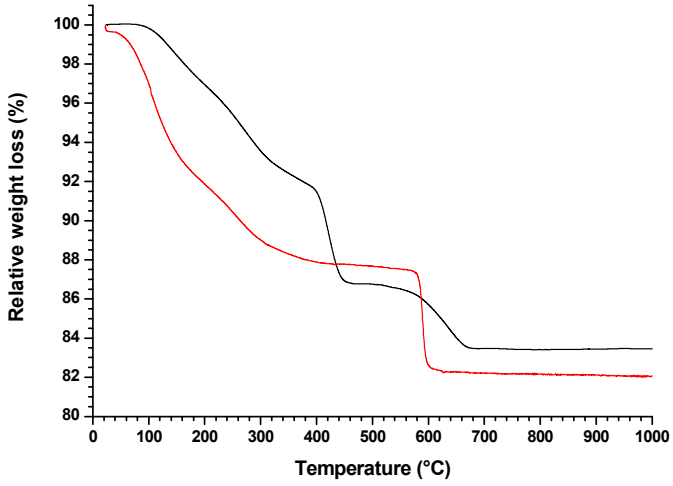

Figure 7. TG analyses performed during the decomposition of U(IV)- (a) and U(VI)-bearing (b) precursors under Ar/H_2 (black) or air (red) atmosphere.

More surprisingly, the relative weight loss measured in oxidative conditions appeared to be higher than that recorded in reducing atmosphere. Indeed, if the dehydration process of uranium(IV) oxide hydrate was found to take place in a similar range of temperature, an additional loss of about 2 to 3% of the initial mass occurred above 400°C. This feature could be correlated to the more efficient elimination of the residual carbon content evidenced in the samples from the TEM observations under air [33]. Moreover, no weight gain correlated to the oxidation of U(IV) was observed. Nevertheless, such phenomenon only accounted for a small weight variation and probably occurred concomitantly to the dehydration process.

On the other hand, the thermograms recorded during the decomposition of U(VI)-bearing precursors appeared more complex owing to the mixture of phases obtained initially. Nevertheless, the various steps observed when heating under reducing conditions fitted well with that reported in the literature for the dehydration then the decomposition of meta-schoepite [30]. Indeed, a first loss of about 8 % was measured up to 400°C and assigned to the successive dehydration of meta-schoepite into related schoepite, then anhydrous schoepite. The second step was recorded from 400 to 450°C and corresponded to the reduction of $UO_3.H_2O$ to U_3O_8, resulting in an additional loss of 5% of the initial mass. Finally, the last transformation, that appeared to occur progressively between 550 and 650°C, was correlated to the complete reduction of uranium as U^{4+}, leading to the formation of UO_2.

As it was observed for $UO_2.H_2O$, the decomposition of U(VI)-bearing precursor in air led to an higher weight mass loss. Again, this result was assigned to the more efficient elimination of residual carbon species under oxidative atmosphere. On this basis, the progressive weight loss observed from room temperature to 500°C probably corresponded to the simultaneous dehydration of the precursor and to the oxidation of uranium(IV) into uranium(VI), leading to the formation of UO_3. The final and sharp weight loss of about 4% evidenced at 600°C was further assigned to the formation of U_3O_8 .

The nature of the uranium oxides obtained after heating at 1000°C (t = 1 hour), either under reducing or oxidative conditions, was further checked by the means of PXRD (Figure 8). As expected from the TGA results, the modification of the operating conditions chosen for the heat treatment allowed us to tailor the O/M ratio in the final samples. Whatever the starting precursor considered, UO_2 was obtained when working under reducing Ar/H_2 atmosphere. For both samples, PXRD patterns exhibited the typical diffraction lines of the well-known fluorite type structure of uranium dioxide. Moreover, Rietveld refinement (Table 1) led to values of the unit cell volume that appeared to be slightly higher than those reported in the literature (typically about 163 $Å^3$ in our study versus 161 $Å^3$ for stoichiometric UO_2 samples [34]). This large value of the lattice could again account for the presence of carbon in the samples, which was not fully eliminated during the calcination step under reducing atmosphere. From these data, the carbon material appears to be directly inserted in the

fluorite-type structure of UO_2, probably as interstitial defects. This result appeared to be in good agreement with the unit cell volumes already reported in the literature for UO_2 samples prepared from metal-organic precursors, such as oxalates, for which the thermal conversion under reducing conditions systematically led to the presence of residual carbon into the lattice [35].

Similarly, heating the precursor in air always led to the preparation of orthorhombic (pseudo-hexagonal) U_3O_8 (space group Amm2) [36]. In this case, the unit cell parameters determined through Rietveld refinement fit well with those reported in the literature (a = 4.148 Å, b = 11.966 Å, c = 6.717 Å [37]), thus excluding the presence of large amounts of impurities inserted in the structure.

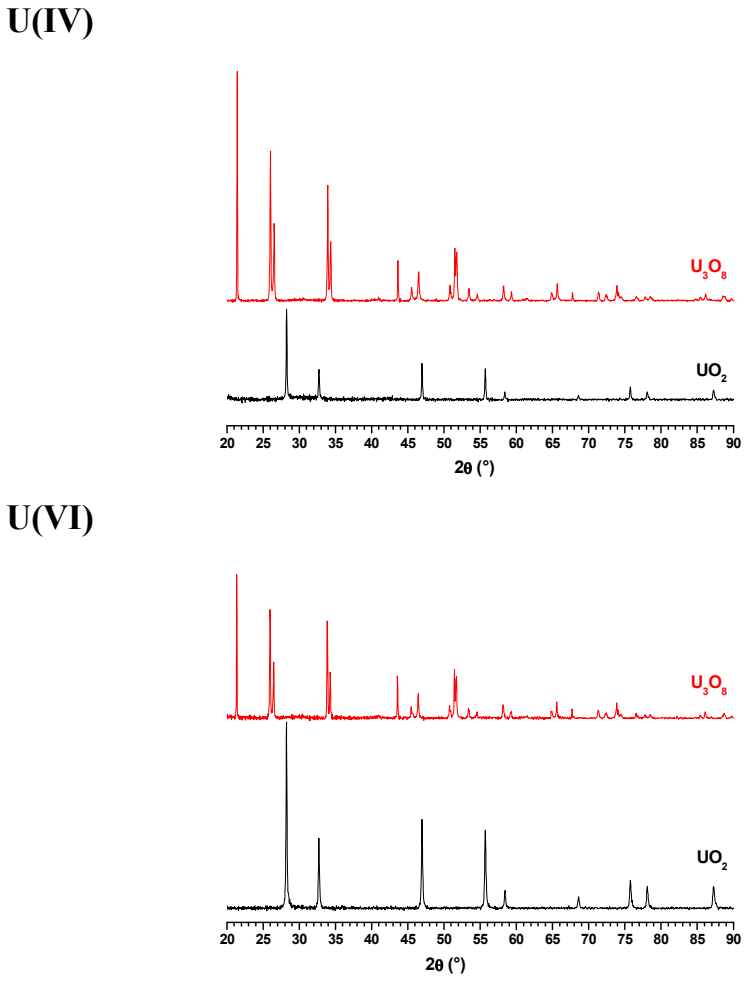

Figure 8. PXRD patterns of the oxide phases obtained from the heat treatment of U-bearing mesospheres at 1000°C under Ar/H_2 (black) or in air (red) atmosphere.

Table 1. Unit cell parameters of the oxide phases obtained after heat treatment at 1000°C.

	Atm.	Compound	a (Å)	b (Å)	c (Å)	V (Å^3)
U(IV)	air	U_3O_8	4.1463(1)	11.9476(3)	6.7207(2)	332.94(2)
	Ar/H_2	UO_2	5.4695(1)	---	---	163.62(1)
U(VI)	air	U_3O_8	4.1454(1)	11.9378(3)	6.7210(2)	332.60(1)
	Ar/H_2	UO_2	5.4671(1)	---	---	163.40(1)

In a last step, the morphology of the powders obtained after heating at high temperature, either under oxidative or reducing atmosphere, was examined by the means of SEM observations (Figure 9). Whatever the starting compound considered, heat treatment under air generally led to significant modifications of the morphology of the powders. Indeed, samples heated at 1000°C for 1 hour did not evidenced any spherical habit but more likely angular grains that already started to sinter. The initiation of this densification step is particularly marked by the formation of numerous grain boundaries. Such important difference compared to the initial shape of U(IV)- and U(VI)-based precursors probably originates from the O/M values in the oxides considered that are frequently associated to an acceleration in the grain growth and sintering kinetics [38]. Indeed, uranium diffusion in orthorhombic U_3O_8 proceeds at rates much faster than in UO_2 [39], with D_U values comparable to that determined in super-stoichiometric $UO_{2.22}$. Such difference in the diffusion coefficients could be as high as 3 orders of magnitude when comparing log D_U at 1500°C for UO_2 and $UO_{2.2}$ [40].

Lower heating temperature must thus be considered to still obtain U_3O_8 mesospheres. Based on the results obtained by TG analyses, additional heat treatments were then performed at 700°C. Despite the important weight loss associated to such operating conditions, they yielded in the pseudomorphic conversion of both U(IV) and U(VI) precursors and to the production of U_3O_8 spherical grains. Nevertheless, these latter exhibited smaller sizes than the initial mesospheres. This trend was limited when starting from U(VI)-based compounds, as the final diameter of the objects was found to be about 220 nm. On this basis, the decomposition associated to the heat treatment probably led to the creation of an important amount of porosity within the sphere and did not result in its densification. Such behaviour was already observed during the conversion of other metal-organic systems into fluorite-type dioxides [41, 42]. Conversely, the samples prepared for U(IV)-bearing precursors presented a significant shrinkage, with a final size close to 60 nm, which might be assigned both to the redox reactions taking place during the conversion leading from UO_2 to U_3O_8, and to the smaller size of the initial grains.

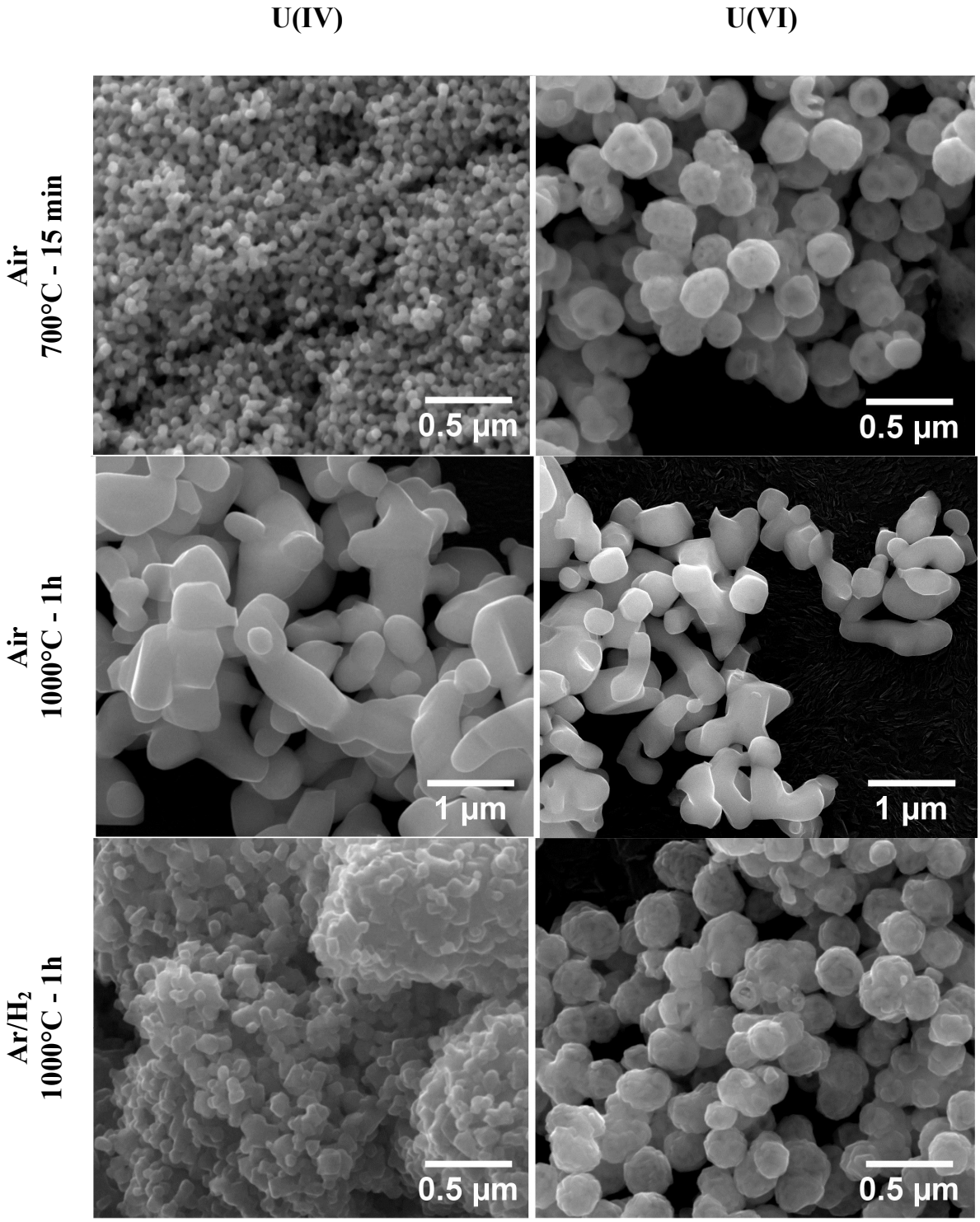

Figure 9. SEM observations of uranium-bearing samples obtained after heating at 700°C or 1000°C under various atmospheres.

Uranium(IV) and uranium(VI)-based mesospheres prepared at low temperature also exhibited different behaviours when heating at high temperature under reducing conditions. Indeed, the conversion of the initial U(VI) precursors, thus their reduction into UO_2, did not cause significant modifications, neither concerning the morphology nor the size. In a similar way to what was observed in air, UO_2 spheres produced thus must present important amounts of porosity. Conversely, the calcination of $UO_2.nH_2O$ precursor resulted in a strong coalescence of the grains. Such phenomenon illustrates the first step of the powder's sintering, which is characterized by the formation of necks between the grains. In this case, the kinetics of bridging must have been fastened by the small size of the grains initially considered, close to 100 nm, which is usually associated to a strong reactivity of the powder then to an important sintering capability. Nevertheless, even if the operating conditions chosen did not allow the preparation of spherical objects, they should probably be obtained by considering lower temperature of calcination.

4. Conclusion

An easy way of synthesis, based on the use of wet chemistry methods, was developed to prepare shape-controlled uranium oxides. In this aim, several precursors were obtained by mixing acidic solutions containing either U^{4+} or UO_2^{2+} cations, with urea acting as a precipitating agent and PEG as surfactant. For several of the experimental conditions explored, either in terms of heating time or temperature, this protocol yielded in the preparation of uranium-based spheres, with sizes varying typically from 50 to 250 nm. In this sense, these objects constitute one of the first shape-controlled actinide compounds with a hierarchical structure reported in the literature.

Moreover, the study of the influence of heating time and temperature allowed to precise the mode of formation of such uranium-based mesospheres, which appeared to depend on the redox state initially considered. On the one hand, for all the conditions studied, U(IV) was found to form from $UO_2.H_2O$ colloids that demonstrated a strong tendency to aggregation. Indeed, the combination of SEM and TEM observations with SAXS measurements revealed a hierarchical organization of the powder with three different scales. The first one corresponded to small crystallites of about 3 nm and acted as the elementary brick of construction. These latter then grouped into spherical agglomerates of 15-20 nm then again aggregate to produce the bigger spheres observed, that can reach up to 200 nm in diameter. On the other hand, the preparation of spherical objects incorporating UO_2^{2+} cations was found to be more dependent on the precipitation conditions. As very distinct morphologies and crystal state were evidenced when varying heating time or temperature, the formation of U(VI)-bearing mesospheres could be considered as a meta-stable form, finally leading to the precipitation of crystalline meta-schoepite.

Finally, the compounds prepared at low-temperature were generally found to present pseudomorphic conversion towards the final high temperature oxides, which still exhibited a spherical habit, provided the conditions of calcination were properly selected. This study thus paves the way to the preparation of a wide variety of shape-controlled actinide oxides. Particularly, the study of thorium-based compounds is now under progress and will provide interesting models exempt from redox reactions.

Acknowledgements

Authors would like to thank J. Nelayah from LMPQ (University Paris 7 Diderot) for his support during the TEM observations. They are also grateful to the Materials Federative Project included in the NEEDS program (Nucléaire, Energie, Environnement, Déchets, Société) of CNRS for its continuous financial support.

References

1. R. Q. Song and H. Colfen, *Adv Mater*, 2010, 22, 1301-1330.
2. T. Wang, D. LaMontagne, J. Lynch, J. Q. Zhuang and Y. C. Cao, *Chem Soc Rev*, 2013, 42, 2804-2823.
3. J. X. Fang, B. J. Ding and H. Gleiter, *Chem Soc Rev*, 2011, 40, 5347-5360.
4. G. J. D. Soler-illia, C. Sanchez, B. Lebeau and J. Patarin, *Chem Rev*, 2002, 102, 4093-4138.
5. L. E. Depero and M. L. Curri, *Curr Opin Solid St M*, 2004, 8, 103-109.
6. A. Trovarelli, *Catal Rev*, 1996, 38, 439-520.
7. E. Y. Pikalova, A. A. Murashkina, V. I. Maragou, A. K. Demin, V. N. Strekalovsky and P. E. Tsiakaras, *Int J Hydrogen Energ*, 2011, 36, 6175-6183.
8. M. Pradhan, S. Sarkar, A. K. Sinha, M. Basu and T. Pal, *Crystengcomm*, 2011, 13, 2878-2889.
9. Q. Wang, G. D. Li, S. Xu, J. X. Li and J. S. Chen, *J Mater Chem*, 2008, 18, 1146-1152.
10. J. E. Kelly, *Progress in Nuclear Energy*, 2014, DOI: doi:10.1016/j.pnucene.2014.02.010.
11. H. H. S. Santana, G. Maier and J. Rodenas, *Appl Radiat Isotopes*, 2011, 69, 1162-1164.
12. E. Remy, S. Picart, S. Grandjean, T. Delahaye, N. Herlet, P. Allegri, O. Dugne, R. Podor, N. Clavier, P. Blanchart and A. Ayral, *J Eur Ceram Soc*, 2012, 32, 3199-3209.
13. H. Daniels, S. Neumeier, A. A. Bukaemskiy, G. Modolo and D. Bosbach, *Progress in Nuclear Energy*, 2012, 57, 106-110.
14. A. Kumar, J. Radhakrishna, N. Kumar, R. V. Pai, J. V. Dehadrai, A. C. Deb and S. K. Mukerjee, *J Nucl Mater*, 2013, 434, 162-169.
15. D. Hudry, C. Apostolidis, O. Walter, T. Gouder, E. Courtois, C. Kubel and D. Meyer, *Chem-Eur J*, 2012, 18, 8283-8287.
16. D. Hudry, C. Apostolidis, O. Walter, T. Gouder, A. Janssen, E. Courtois, C. Kubel and D. Meyer, *Rsc Adv*, 2013, 3, 18271-18274.
17. N. Dacheux, V. Brandel and M. Genet, *New J Chem*, 1995, 19, 1029-1036.
18. N. Dacheux, V. Brandel and M. Genet, *New J Chem*, 1995, 19, 15-25.
19. F. Clarens, J. De Pablo, I. Diez-Perez, I. Casas, J. Gimenez and M. Rovira, *Environ Sci Technol*, 2004, 38, 6656-6661.
20. S. F. Wang, F. Gu, C. Z. Li and H. M. Cao, *J Cryst Growth*, 2007, 307, 386-394.
21. N. Dacheux, N. Clavier and J. Ritt, *J Nucl Mater*, 2006, 349, 291-303.
22. P. Thompson, D. E. Cox and J. B. Hastings, *Journal of Applied Crystallography*, 1987, 20, 79-83.

23. C. Frontera and J. Rodriguez-Carvajal, *Physica B: Condensed Matter*, 2003, 335, 219-222.
24. Y. H. Wang, M. Frutschi, E. Suvorova, V. Phrommavanh, M. Descostes, A. A. A. Osman, G. Geipel and R. Bernier-Latmani, *Nat Commun*, 2013, 4.
25. H. M. Wu, Y. G. Yang and Y. C. Cao, *J Am Chem Soc*, 2006, 128, 16522-16523.
26. G. N. Nikovskaya, Z. R. Ul'berg and N. P. Strizhak, *Colloid J+*, 2002, 64, 172-177.
27. P. C. Debets and B. O. Loopstra, *J Inorg Nucl Chem*, 1963, 25, 945-953.
28. C. Y. Lin, Y. C. Yeh and P. R. Griffiths, *J Radioan Nucl Ch Ar*, 1989, 131, 131-137.
29. R. J. Finch, M. A. Cooper, F. C. Hawthorne and R. C. Ewing, *Can Mineral*, 1996, 34, 1071-1088.
30. R. J. Finch, F. C. Hawthorne and R. C. Ewing, *Can Mineral*, 1998, 36, 831-845.
31. M. T. Hutchings, *J Chem Soc Farad T 2*, 1987, 83, 1083-1103.
32. J. S. Pedersen, *Adv Colloid Interfac*, 1997, 70, 171-210.
33. L. De Almeida, S. Grandjean, N. Vigier and F. Patisson, *Eur J Inorg Chem*, 2012, 31, 4986-4999.
34. B. Wasserstein, *Nature*, 1951, 168, 380-380.
35. S. Hubert, J. Purans, G. Heisbourg, P. Moisy and N. Dacheux, *Inorg Chem*, 2006, 45, 3887-3894.
36. R. Herak, *Acta Crystall B-Stru*, 1969, B 25, 2505-&.
37. B. O. Loopstra, *Acta Crystallogr*, 1964, 17, 651-&.
38. H. Assmann, W. Dorr and M. Peehs, *J Nucl Mater*, 1986, 140, 1-6.
39. D. G. Leme and H. Matzke, *J Nucl Mater*, 1983, 115, 350-353.
40. H. Matzke, *J Nucl Mater*, 1969, 30, 26-&.
41. L. Claparede, N. Clavier, N. Dacheux, A. Mesbah, J. Martinez, S. Szenknect and P. Moisy, *Inorg Chem*, 2011, 50, 11702-11714.
42. L. Claparede, N. Clavier, N. Dacheux, P. Moisy, R. Podor and J. Ravaux, *Inorg Chem*, 2011, 50, 9059-9072.